Multiport Network Description and Radiation Characteristics of Coupled Dielectric Resonator Antennas

Gregory P. Junker, *Member, IEEE*, Ahmed A. Kishk, *Fellow, IEEE*, and Allen W. Glisson, *Senior Member, IEEE*

***Abstract*—An efficient procedure is presented to investigate the mutual coupling effects and radiation characteristics of dielectric resonator (DR) antennas operating in an array environment. The procedure is based on the method of moments (MoM) as applied to a system of surface integral equations (SIE's) for the coupling of a dielectric body of revolution (BOR) to a nonBOR geometry. The antenna array elements are situated on a ground plane and fed by coaxial probes. Multiport network impedance parameters computed by this method show good agreement with those obtained by measurement. Computed driving point impedances are given for arrays exhibiting optimum pattern performance in terms of low cross polarization and good pattern symmetry.**

***Index Terms*— Dielectric antennas.**

I. Introduction

SINCE the early experimental studies to determine the radiation characteristics of dielectric resonator (DR) antennas [1], [2] and the numerical evaluation of several of the lowest source-free modes of cylindrical DR's situated in free-space [3], [4] there has been continued interest in the development of DR antennas. Recently, it has been experimentally established that DR's are effective as antenna array elements [5]. To date, most numerical modeling for DR antennas has been focused on single elements [6]. By use of a single-mode approximation together with reaction concepts, the mutual coupling between each element of a two-element array of hemispherical DR antennas was theoretically investigated [7]. Even upon replacing the single-mode approximation with a full modal expansion, this technique is limited to spherical bodies since it utilizes the Green's function for a current element located vertically inside a dielectric sphere. In order to completely characterize an antenna array, the design engineer must have at his disposal a tool that takes into account all mutual coupling effects. This is especially important for large phased arrays where the effects of mutual coupling can cause significant impedance variation with scan angle as well as introduce blindness effects [8]. A rigorous numerical model based upon the method of moments (MoM) was introduced in [9] to determine the driving point impedances and radiation patterns of ground-plane-backed linear arrays of rotationally symmetric DR elements. Simple methods such as the electromagnetic force (EMF) method may not be suitable for the study of mutual coupling effects. Indeed, it has already been established that the EMF method is not of sufficient accuracy to determine self and mutual impedances [10] of antenna arrays since it is in fact merely an integral identity and not directly related to the currents at the driving points of the antenna [11].

In this paper, a procedure is presented for the accurate characterization of a linear array of coaxial probe fed DR elements in terms of its multiport impedance, admittance, or scattering matrix. These antenna arrays should find utility in tracking and supergain applications because of the DR's high power handling capability and low loss, which is of special concern in millimeter wave applications.

Manuscript received January 16, 1996; revised November 8, 1996. This work was supported in part by the National Science Foundation grant ECS-9 015 328.

The authors are with the Department of Electrical Engineering, University of Mississippi, University, MS 38677 USA.

Publisher Item Identifier S 0018-926X(98)02271-6.

II. Formulation

A. The Field Equivalences

The electromagnetic field equivalence principle [12] is used to obtain a system of surface integral equations (SIE's) similar to the body of revolution (BOR) formulation of [13], for composite radiators consisting of N homogeneous regions, each of which may have embedded wires. The generalized geometry for such a radiator is illustrated in Fig. 1. The whole space is divided into $N+1$ homogeneous regions with permittivities ϵ_i and permeabilities μ_i for $i = 0, 1, 2, \cdots, N$. Each region V_i is surrounded by a closed-surface S_i and is associated with an inward normal unit vector $\boldsymbol{n}_i$. The surface interface between regions V_i and V_j is $S_{ij}, i \neq j$. Thus, S_i is the set of all interface surfaces S_{ij}, where j represents all region numbers that interface with region V_i. Note that the surface $S_{ij} = S_{ji}$; however, the normal unit vectors $\boldsymbol{n}_i$ and $\boldsymbol{n}_j$ are in opposite directions to each other on S_{ij}. The total fields in each region are denoted by $\boldsymbol{E}_i$ and $\boldsymbol{H}_i$, where $i = 0, 1, 2, \cdots, N$ for the electric and magnetic fields, respectively. The time variation $e^{j\omega t}$ is assumed and suppressed throughout. The total fields in each region are the fields due to the equivalent currents surrounding this region plus the fields due to the impressed current sources. From Maxwell's equations, and the equivalence principle, one can express the field in each region in terms of unknown electric and magnetic equivalent surface currents.

0018–926X/98$10.00 © 1998 IEEE

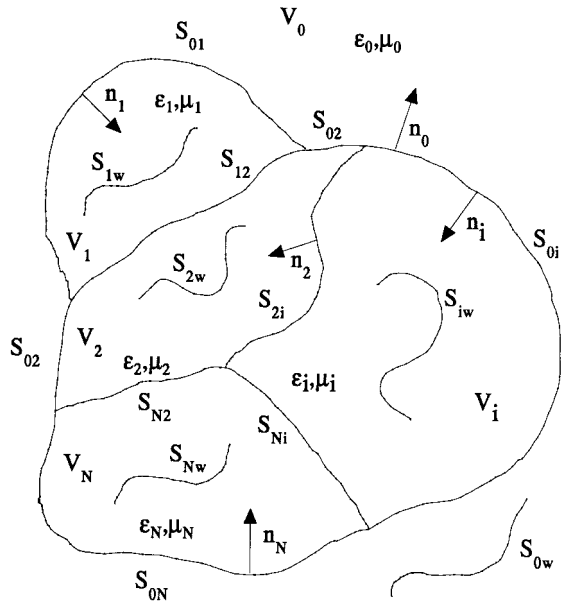

Fig. 1. General geometry of the composite dielectric body with embedded wires.

According to the equivalence principle, the original problem can be decomposed into a number of auxiliary problems that are equal to the number of dielectric regions. To obtain the ith auxiliary problem, the boundaries of the region V_i are replaced by equivalent surface currents radiating in a homogeneous medium with the constitutive parameters of region V_i. Electric currents are used for the embedded wire surfaces and equivalent electric and magnetic currents are used for the dielectric boundaries. The electric and magnetic currents appearing on opposite sides of a dielectric interface in different auxiliary problems are taken equal in magnitude and opposite in direction to assure continuity of the tangential components of the fields on these boundaries as they were continuous in the original problem. In this procedure, the fields produced within the region boundaries by the equivalent currents are the same as those in the original problem, while the zero field is produced outside these boundaries. The electric and magnetic surface currents along S_i are

$$\boldsymbol{J}_i = \boldsymbol{n}_i \times \boldsymbol{H}_i \tag{1}$$

$$\boldsymbol{M}_i = -\boldsymbol{n}_i \times \boldsymbol{E}_i. \tag{2}$$

The unknown surface electric current on the embedded wires is directed along its surface S_{iw} and is denoted as $\boldsymbol{J}_{iw}$. By enforcing the boundary conditions of continuity of tangential components of the electric field on the wire surface as

$$\boldsymbol{E}_{iw}|_{\tan} = 0 \quad \text{on} \quad S_{iw} \tag{3}$$

and continuity of both the tangential components of the electric and magnetic fields on the dielectric surfaces as

$$\boldsymbol{E}_i|_{\tan} = \boldsymbol{E}_j|_{\tan} \quad \text{on} \quad S_{ij} \tag{4}$$

$$\boldsymbol{n}_i \times \boldsymbol{H}_i = \boldsymbol{n}_i \times \boldsymbol{H}_j \quad \text{on} \quad S_{ij} \tag{5}$$

a system of surface integrodifferential equations can be written in an operator form in terms of the equivalent surface currents as

$$\boldsymbol{E}_i(\boldsymbol{J}_i + \boldsymbol{J}_{iw}, \boldsymbol{M}_i)|_{\tan} = -\boldsymbol{E}_i(\boldsymbol{J}_i^{\text{inc}}, \boldsymbol{M}_i^{\text{inc}})|_{\tan} \quad \text{on} \quad S_{iw} \tag{6}$$

$$\begin{aligned}[\boldsymbol{E}_i(\boldsymbol{J}_i + \boldsymbol{J}_{iw}, \boldsymbol{M}_i) + \boldsymbol{E}_j(\boldsymbol{J}_j + \boldsymbol{J}_{jw}, \boldsymbol{M}_j)]_{\tan} \\ = [\boldsymbol{E}_j(\boldsymbol{J}_j^{\text{inc}}, \boldsymbol{M}_j^{\text{inc}}) - \boldsymbol{E}_i(\boldsymbol{J}_i^{\text{inc}}, \boldsymbol{M}_i^{\text{inc}})]_{\tan} \quad \text{on} \quad S_{ij}\end{aligned} \tag{7}$$

$$\begin{aligned}\boldsymbol{n}_i \times [\boldsymbol{H}_i(\boldsymbol{J}_i + \boldsymbol{J}_{iw}, \boldsymbol{M}_i) + \boldsymbol{H}_j(\boldsymbol{J}_j + \boldsymbol{J}_{jw}, \boldsymbol{M}_j)] \\ = \boldsymbol{n}_i \times [\boldsymbol{H}_j(\boldsymbol{J}_j^{\text{inc}}, \boldsymbol{M}_j^{\text{inc}}) - \boldsymbol{H}_i(\boldsymbol{J}_i^{\text{inc}}, \boldsymbol{M}_i^{\text{inc}})] \quad \text{on} \quad S_{ij}.\end{aligned} \tag{8}$$

The above system of equations is known as the E-PMCHW formulation [14]. The integrodifferential operators $\boldsymbol{E}(\boldsymbol{J}, \boldsymbol{M})$ and $\boldsymbol{H}(\boldsymbol{J}, \boldsymbol{M})$, are defined in terms of the magnetic and electric vector and scalar potential functions [12]. The arguments $\boldsymbol{J}_i^{\text{inc}}$ and $\boldsymbol{M}_i^{\text{inc}}$ represent the incident electric and magnetic currents in region i, respectively.

B. Moment Method Solution

The coupled system of SIE's (6)–(8) are to be specialized to dielectric bodies such that the regions V_i are delineated by surfaces of revolution. These coupled equations are then numerically solved by employing a Galerkin MoM procedure [15]. In the free-space equivalent problem, the antenna geometry (excluding the embedded wires) is defined by a surface of revolution swept out by rotating a generating arc about the body's symmetry axis. Due to this symmetry, two components of equivalent electric and magnetic currents can be identified: one directed along the generating arc, i.e., the $\boldsymbol{t}$ component, and the other in the circumferential direction, i.e., the $\boldsymbol{\phi}$ component. Hence, the unknown currents on the BOR are modeled as harmonic $(e^{jn\phi})$ entire domain expansion functions for the circumferential variation, where n is the nth Fourier mode and as piecewise linear subdomain functions for the dependence on axial curvature. The unknown equivalent current on the wires, in this case the actual currents, are modeled as piecewise linear subdomain functions. After application of the Galerkin procedure to the above system of equations, the resulting matrix equation is of the form as in (9), shown at the bottom of the next page. The vectors $|JM\rangle_n$ represent the electric and magnetic current coefficients for the nth Fourier mode of the basis functions, which reside on surface S_i and are given as

$$\begin{bmatrix} |J_i\rangle \\ |M_i\rangle \end{bmatrix}_n. \tag{10}$$

Since the surface S_i is the sum of all the boundaries S_{ij} of region V_i where $i \neq j$ and, since j represents all the region numbers adjacent to the region V_i, the equivalent current $\boldsymbol{J}_i$ is given as

$$\boldsymbol{J}_i = \sum_j \boldsymbol{J}_{ij} \quad \text{on the boundaries of } V_i \tag{11}$$

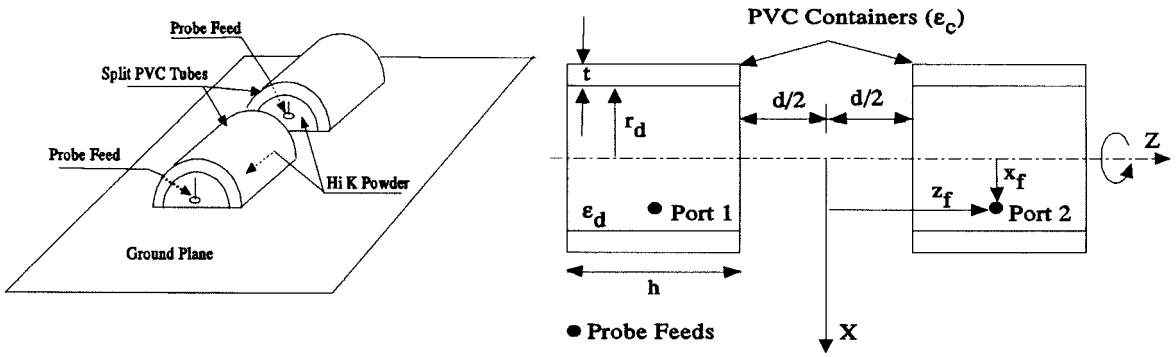

(a) (b)

Fig. 2. Geometry of the test array. (a) The two-element array of half-split CDR's. (b) The coordinate system.

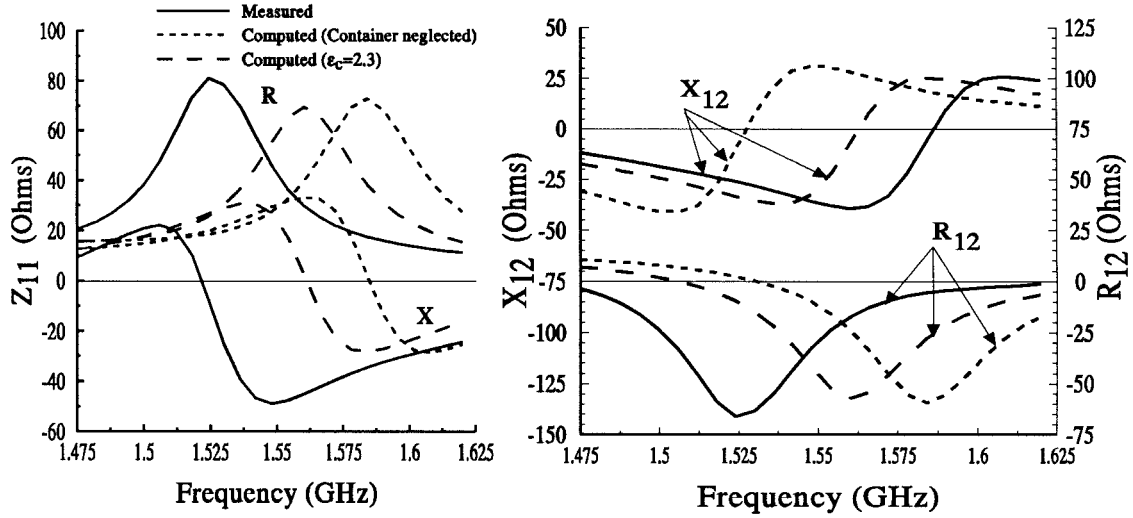

(a) (b)

Fig. 3. Measured and computed self and mutual impedances versus frequency for the antenna of Fig. 2(a) with $r_d = 24.5$ mm, $h = 39.5$ mm, $t = 4.2$ mm, $d = 16$ mm, $x_{f1} = x_{f2} = 14.4$ mm, $z_{f1} = -27.75$ mm, $z_{f2} = 27.75$ mm. (a) Z_{11}. (b) Z_{12}.

and is given similarly for $\boldsymbol{M}_i$. The vector $|J_w\rangle$ represents the current expansion coefficients for the currents $\boldsymbol{J}_{iw}$ that reside on the wire surface S_{iw}. The large square submatrix involving the partitions $[BB]$ represent the inner products in the Galerkin procedure for the case that the testing and basis functions are on the surface S_{ij}. The banded nature of this part of the matrix is due to the orthogonality of the exponential function $e^{jn\phi}$. The partitioned row matrix comprising the submatrices $[WB]$ and the partitioned column matrix comprising the submatrices $[BW]$ represent inner products resulting from the Galerkin procedure when the testing functions are on S_{ij} and the basis functions are on S_{iw} for $[BW]$ and vice versa for $[WB]$. The square matrix $[WW]$ represents the results of the Galerkin procedure when both the testing and basis functions are on S_{iw}. Additional details for these definitions can be found in [6] and details about the matrix elements can be found in [16]. The extended delta source [17] is used to model the impressed (incident) electric field to get the right-hand side of (9).

$$\begin{bmatrix} [BB]_{-n} & \cdot & \cdots & \cdot & \cdots & \cdot & \cdot & [BW]_{-n} \\ \cdot & [BB]_{-n+1} & \cdots & \cdot & \cdots & \cdot & 0 & [BW]_{-nn+1} \\ \cdot & \cdot & \cdots & \cdots & \cdots & \cdots & \cdots & \cdots \\ \cdot & \cdot & \cdots & [BB]_0 & \cdots & \cdot & \cdot & [BW]_0 \\ \cdot & 0 & \cdots & \cdot & \cdots & \cdots & \cdot & \cdots \\ \cdot & \cdot & \cdots & \cdot & \cdots & [BB]_{n-1} & \cdot & [BW]_{n-1} \\ \cdot & \cdot & \cdots & \cdots & \cdot & \cdot & [BB]_n & [BW]_n \\ [WB]_{-n} & [WB]_{-n+1} & \cdots & [WB]_0 & \cdots & [WB]_{n-1} & [WB]_n & [WW] \end{bmatrix} \begin{bmatrix} |JM\rangle_{-n} \\ |JM\rangle_{-n+1} \\ \cdots \\ |JM\rangle_0 \\ \cdots \\ |JM\rangle_{n-1} \\ |JM\rangle_n \\ |J_w\rangle \end{bmatrix} = \begin{bmatrix} |0\rangle \\ |0\rangle \\ \cdots \\ |0\rangle \\ \cdots \\ |0\rangle \\ |0\rangle \\ |V_w\rangle \end{bmatrix} \tag{9}$$

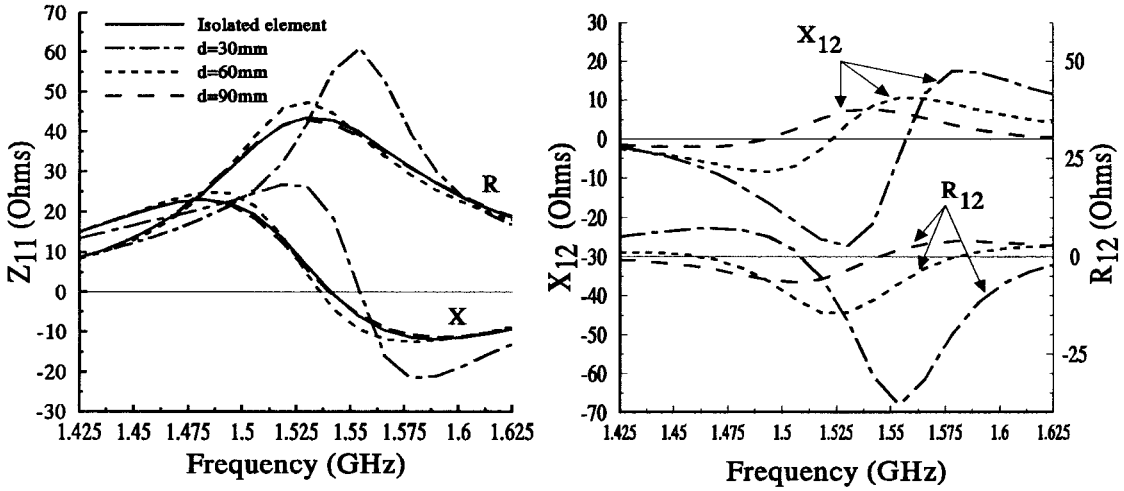

(a) (b)

Fig. 4. Computed self and mutual impedances for various spacings d versus frequency for the antenna of Fig. 2(a) with $r_d = 24.5$ mm, $h = 39.5$ mm, $t = 0.0$ mm, $x_{f1} = x_{f2} = 14.4$ mm, $z_{f1} = -(27.75 + d/2)$ mm, $z_{f2} = (27.75 + d/2)$ mm. (a) Z_{11}. (b) Z_{12}.

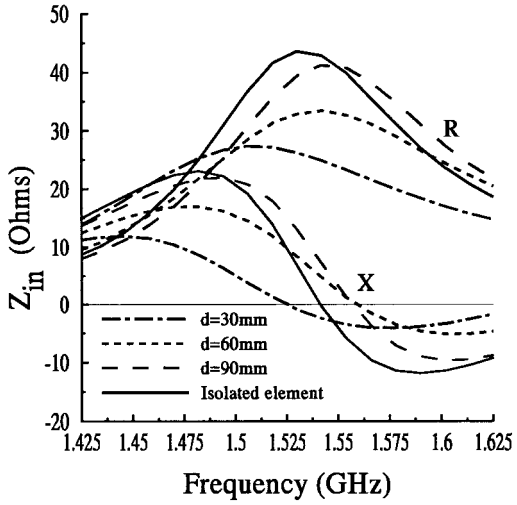

Fig. 5. Computed driving point impedances for various spacings d versus frequency for the antenna of Fig. 2(a) with $r_d = 24.5$ mm, $h = 39.5$ mm, $t = 0.0$ mm, $x_{f1} = x_{f2} = 14.4$ mm, $z_{f1} = -(27.75 + d/2)$ mm, $z_{f2} = (27.75 + d/2)$ mm.

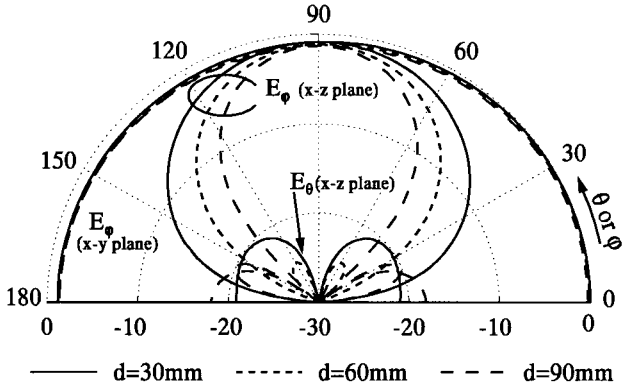

Fig. 6. Computed principal plane patterns for the antenna array of Fig. 2(a) with $r_d = 24.5$ mm, $h = 39.5$ mm, $t = 0.0$ mm, $x_{f1} = x_{f2} = 14.4$ mm, $z_{f1} = -(27.75+d/2)$ mm, $z_{f2} = (27.75+d/2)$ mm, $V_{p1} = V_{p2} = 1\angle 0°$.

Since the quantity of interest is the short-circuit admittance matrix, the procedure described in [6] is used to obtain the current on the wires. Once the current on the wires is found, the current on the dielectric surfaces can be obtained. These currents can then be used to determine the radiation characteristics of the antenna in region V_0. Available in the literature are expressions for the elements of $[BW]$ and $[WB]$ [6], as well as $[WW]$ [18].

The most direct way to obtain the multiport network description of the antenna array from the MoM model is to determine the short-circuit multiport admittance matrix $[\boldsymbol{Y}]$. The elements of the admittance matrix can be determined by driving the pth port with the appropriate voltage source while the remaining elements are treated as parasitic, i.e., their input terminals are short circuited. The admittance matrix elements are given as $Y_{pi} = J_p/V_i|_{V_{j=0}}$ for $j = 1, 2, \cdots, N_w$ and $j \neq p$. After obtaining the elements of $[\boldsymbol{Y}]$, other network descriptions such as the open circuit impedance matrix $[Z]$ and the scattering matrix $[S]$ can be obtained from basic microwave network theory [19].

III. Numerical Results

A. Experimental Verification

Since it has been established that a half-split cylindrical dielectric resonator (CDR) can support a variety of desirable quasi-TE modes [20], it should prove advantageous in an array environment and, as such, it is the element of choice for the test antenna. It has been shown that careful fabrication procedures must be employed in order to build a test antenna which can be used to verify theoretical models of DR antennas. Therefore, the techniques presented in [21] were employed to construct the test array. The antenna under consideration, together with its coordinate system, is illustrated in Fig. 2(a) and (b), respectively. This antenna consists of two half-split PVC tubes of length $h = 39.5$ mm, radius $r = 24.5$ mm, and wall thickness $t = 4.2$ mm displaced on the z axis by a distance $d = 16$ mm. Each end of the tube is closed by a thin half-circular disk of clear butyrate sheet stock and filled

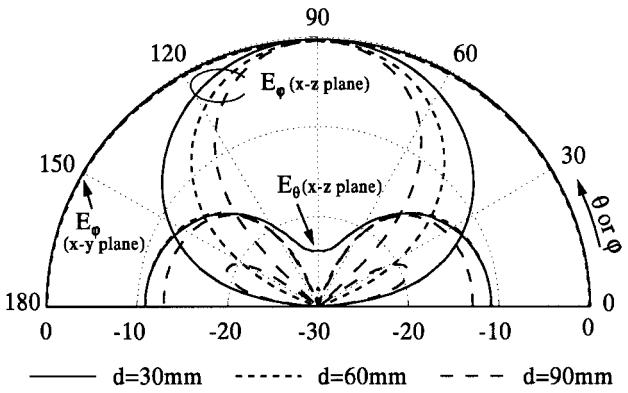

Fig. 7. Computed principal plane patterns for the antenna array of Fig. 2(a) with $r_d = 24.5$ mm, $h = 39.5$ mm, $t = 0.0$ mm, $x_{f1} = 14.4$ mm, $x_{f2} = -14.4$ mm, $z_{f1} = -(27.75 + d/2)$ mm, $z_{f2} = (27.75 + d/2)$ mm, $V_{p1} = 1\angle 0°, V_{p2} = 1\angle 180°$.

with Emerson & Cumin Hi-K dielectric powder of relative permittivity $\epsilon_d = 12.0$. The powdered material was used to ensure that all conducting parts of the antenna were in good mechanical contact with the dielectric material. All plastic components were fixed in position with silicone adhesive. The TE_{01} mode was excited by operating at its resonant frequency and choosing the proper coaxial probe position [20]. The TE_{01} mode was chosen because of the desire to fabricate two elements that were essentially identical. Use of elements with identical characteristics reduces experimental errors. To excite this broadside mode, the 0.381-mm radius coaxial feed probes, which extend 15 mm from the top of the ground plane into the dielectric material, are positioned at $x_f = 14.4$ mm and $z_f = +27.75$ mm. Precision 3.5 mm connectors with solder pot contacts are used to connect the coaxial probe to an HP8510B network analyzer.

The half-split CDR's of Fig. 2(a), can be treated as axisymmetric by invoking image theory and removing the ground plane. The parameters of the two-element array are shown in Fig. 2(b). Doing so results in full CDR's in free-space each excited by a thin wire dipole. Fig. 3(a) and (b) plots the measured and computed self and mutual impedances, respectively, for the experimental array as a function of frequency. It should be mentioned that one element was driven and the other was terminated by a 50-Ω load. The electrical length of the 3.5-mm connector was taken into consideration as a result of the full two-port Hewlett-Pakard calibration procedure. Since the measured data for Z_{11} and Z_{22} exhibited overlay agreement when plotted, only measured data for Z_{11} is presented. In all the numerical models presented in this paper, 19 basis functions per dielectric wavelength were used to model the feed probe and the -3 to $+3$ Fourier azimuthal modes were found to be adequate to ensure convergence. Two different numerical models were considered. The first model completely neglected the presence of the container while the second modeled the PVC container and neglected the butyrate sheet stock. The numerical model, which neglects the presence of the PVC container, indicates that there is a peak in the resistive part of the self impedance near 1.584 GHz, which is 3.9% higher than that of the test array where the resistive peak occurs near 1.524 GHz. However, upon modeling the PVC container with a dielectric constant of 2.3, the frequency at which the peak of the real part of the self impedance occurs dropped to 1.56 GHz, which is only 2.6% higher than that measured. The levels of the computed self impedance varied only slightly upon introduction of the PVC container into the numerical model. This result indicates that the PVC container, which could represent a protective cover cannot always be neglected in the numerical model, even though its dielectric constant is low. This is especially true when the feed probe is in close proximity to the "walls" of the resonator. Since the resistive part of the self impedance is directly related to the radiation resistance and peaks at the frequency that results in maximum radiated power, mutual coupling effects should be the strongest at this frequency. Hence, as expected, the peak of the mutual resistances (though negative) occur at the same frequencies as that of the self-resistance peaks, as indicated in Fig. 3(b). Though not very meaningful by themselves, it is interesting to note that for these closely spaced DR elements, the self and mutual impedances are of approximately the same order of magnitude thus indicating very strong coupling.

B. Numerical Study

To numerically investigate the effects of mutual coupling upon terminal parameters and radiation characteristics of the test array, the distance between the array elements was increased from 16 to 30, 60, and 90 mm, respectively. It should be pointed out that the "container" that encased the dielectric material of relative permittivity $\epsilon_d = 12$ was neglected in the numerical study. Fig. 4(a) shows the self impedances plotted as a function of frequency for various element spacings when the other element is passive together with the input impedance of an isolated element. As can be seen from the figure, the self impedances (in this case, the driving point impedance for the active element in the presence of a parasite) for spacings of 60 and 90 mm exhibit only a small change in frequency response from the driving point impedance of the isolated element. This is not to say, however, that the effect of mutual coupling can be ignored for these element spacings when modeling the array in terms of its microwave multiport impedance matrix. As can be seen from Fig. 4(b), the mutual impedances are not insignificant and, therefore, cannot be neglected when determining the driving point impedances when both elements are active. Fig. 5 plots the driving point impedances for the two-element array when $V_{p1} = V_{p2} = 1\angle 0^0 V$. As can be seen, the driving point impedances for spacings of 60 and 90 mm are no longer in good agreement with each other or with the input impedance of the isolated element. Note that the array resonant frequency, as determined by the peak of the driving point resistances, increases upon increasing element spacing from 30 to 60 mm and then begins to decrease toward that of an isolated element when the separation distance was increased to 90 mm. Fig. 6 shows the principal patterns for the two-element array with both element ports driven in phase and operating at 1.5 GHz for various element spacings. Since this configuration results in an H-plane array, as expected, the E-plane pattern (E_ϕ, x-y plane) is essentially unchanged throughout the spacing range;

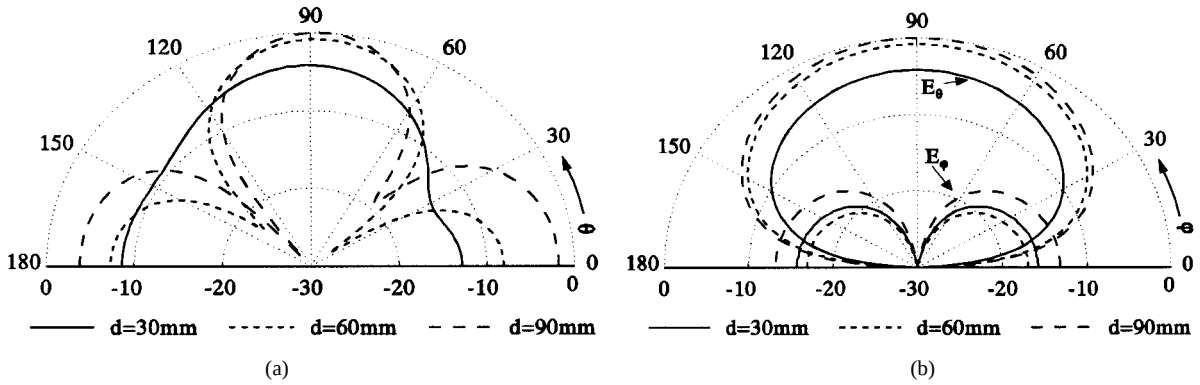

Fig. 8. Computed principal plane patterns for the antenna array of Fig. 2(a) with $r_d = 24.5$ mm, $h = 39.5$ mm, $t = 0.0$ mm, $x_{f1} = x_{f2} = 0.0$ mm, $z_{f1} = -(6.0 + d/2)$ mm, $z_{f2} = (33.5 + d/2)$ mm, $V_{p1} = V_{p2} = 1\angle 0°$. (a) E_θ (y-z plane). (b) E_θ and E_ϕ (x-y plane).

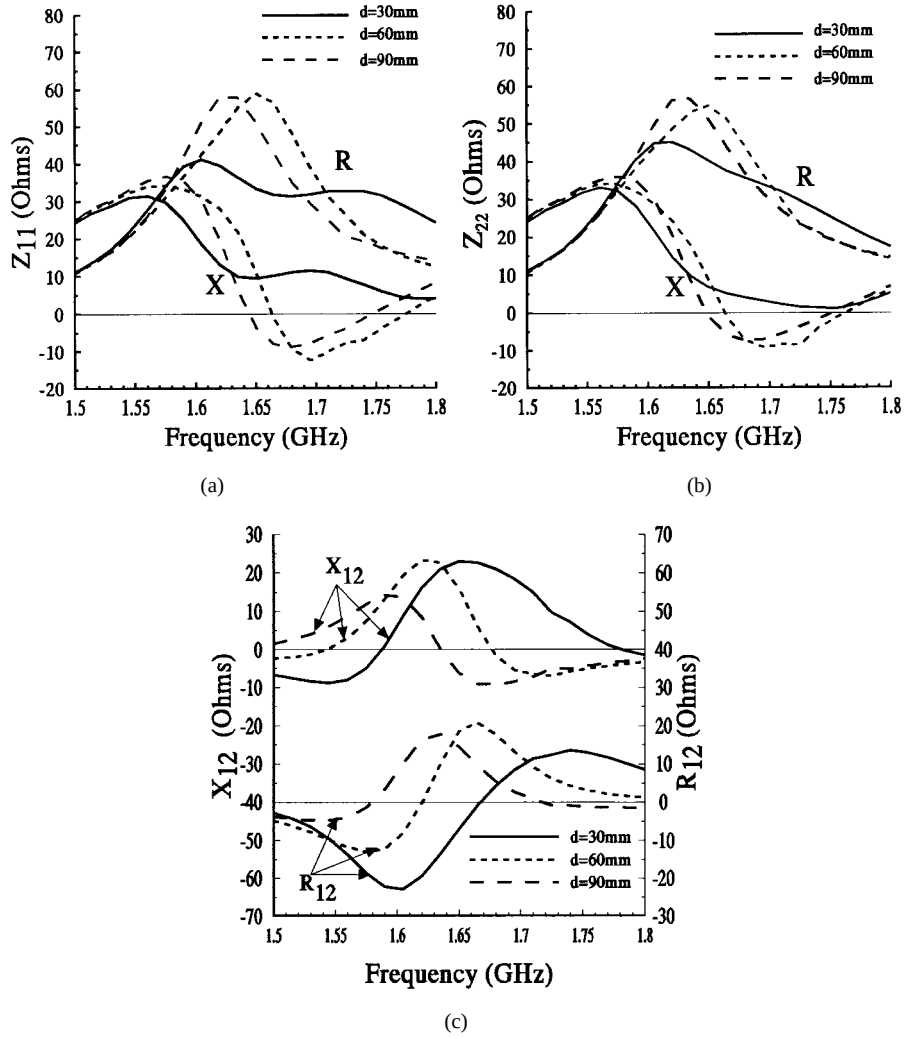

Fig. 9. Computed self and mutual impedances for various spacings d versus frequency for the antenna of Fig. 2(a) with $r_d = 24.5$ mm, $h = 39.5$ mm, $t = 0.0$ mm, $x_{f1} = x_{f2} = 0.0$ mm, $z_{f1} = -(6.0 + d/2)$ mm, $z_{f2} = (33.5 + d/2)$ mm. (a) Z_{11}. (b) Z_{22}. (c) R_{12} and X_{12}.

however, there is some E-plane pattern asymmetry due to the presence of weak high-order modes. Upon increasing element separation, it is noted that E_ϕ in the H plane (y-z plane) becomes more directive and sidelobes appear at the 90-mm spacing. The cross-polar component E_θ decreases upon increasing the element spacing from 30 to 60 mm and then increases upon the appearance of sidelobes at the spacing of 90 mm. To further investigate the slight lack of symmetry, the positions of the feed probes were changed so that the probe at port 1 was positioned at $x_f = -14.4$ mm and driven 180° out of phase from the feed probe at port 2. As seen from Fig. 7, this effectively cancels higher order modes and results

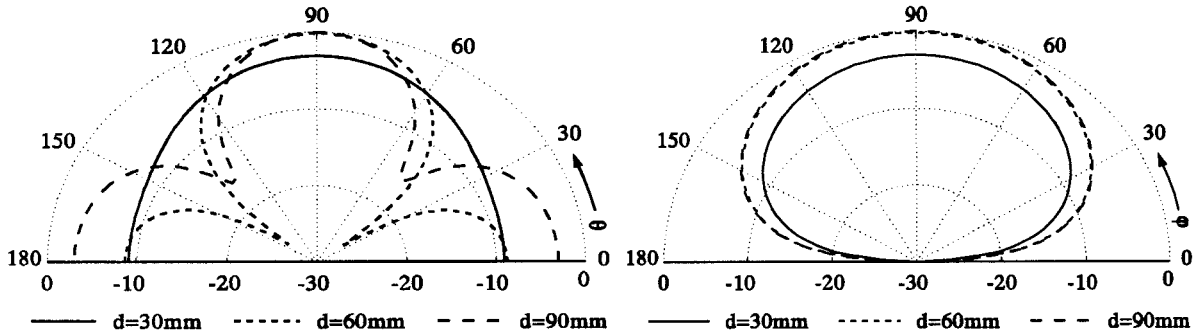

Fig. 10. Computed principal plane patterns for the antenna array of Fig. 2(a) with $r_d = 24.5$ mm, $h = 39.5$ mm, $t = 0.0$ mm, $x_{f1} = x_{f2} = 0.0$ mm, $z_{f1} = -(33.5 + d/2)$ mm, $z_{f2} = (33.5 + d/2)$ mm, $V_{p1} = 1\angle 0°, V_{p2} = 1\angle 180°$. (a) E_θ (y-z plane). (b) E_θ and E_ϕ (x-y plane).

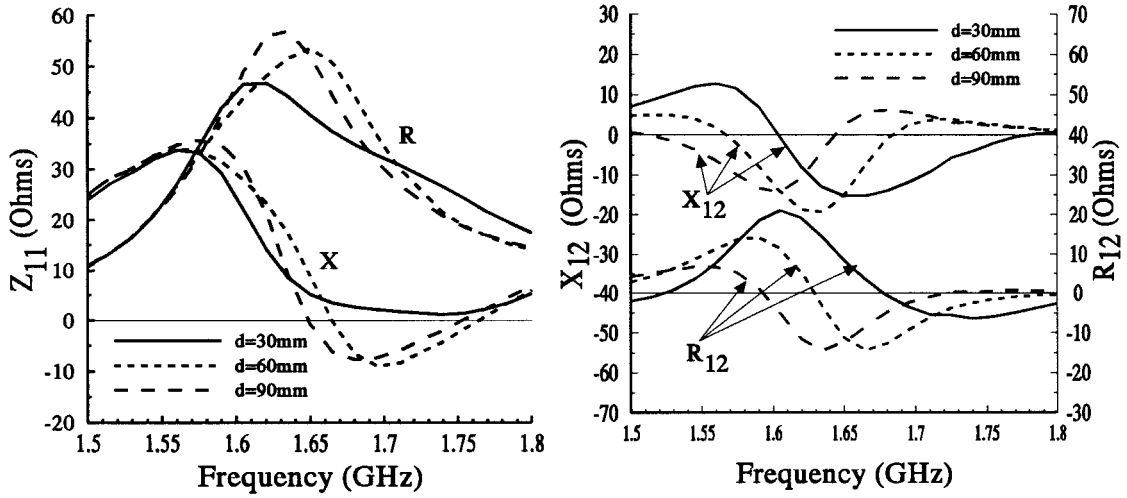

Fig. 11. Computed self and mutual impedances for various spacings d versus frequency for the antenna of Fig. 2(a) with $r_d = 24.5$ mm, $h = 39.5$ mm, $t = 0.0$ mm, $x_{f1} = x_{f2} = 0.0$ mm, $z_{f1} = -(33.5 + d/2)$ mm, $z_{f2} = (33.5 + d/2)$ mm. (a) Z_{11}. (b) Z_{12}.

in a symmetric E-plane pattern. However, the cross-polar components for all three element spacings have increased. The cross polarization increased because the feed probes are not situated in the same plane and, as such, they couple to modes having undesirable characteristics.

The TE_{01} mode can also be excited to create an E-plane array with these elements for an axisymmetric array. This can be accomplished for the spacing $d = 30$ mm by positioning the feed probes at $x_{f1} = x_{f2} = 0.0$ mm, $z_{f1} = -21.0$ mm, and $z_f 2 = 48.5$ mm and driving both ports in phase. Fig. 8(a) is a plot of the E-plane patterns (E_θ in the y-z plane) and Fig. 8(b) is a plot of the H-plane patterns (E_θ in the x-y plane) and the cross-polarization patterns (E_ϕ in the x-y plane). The array is operating at 1.7 GHz for element spacings of $d = 30$, 60, and 90 mm along the z axis. Note that there is a lack of symmetry in the E-plane patterns for all element spacings. This asymmetry is caused by coupling of modes other than the dominant TE_{01} mode. Fig. 9(a) and (b) show Z_{11} and Z_{22}, respectively, and Fig. 9(c) shows R_{12} and X_{12}. As can be seen from Fig. 9(a) and (b) Z_{11} and Z_{22} are not the same. Since the frequencies at which the peaks of the self resistances occur are spread over a certain range of frequencies, it may be possible to increase the impedance bandwidth of an antenna by intentionally causing the peaks of R_{11} and R_{22} to occur at slightly different frequencies. However, given that the pattern is of primary concern, this observation concerning impedance bandwidth may not always prove fruitful. To alter the array to operate as a symmetric array and yield a broadside pattern, the feed probes are positioned at $z_f = \pm 48.5$ mm and the two ports are driven 180° out of phase. The principle plane patterns are given in Fig. 10(a) for E_θ in the y-z plane and in Fig. 10(b) for E_θ in the x-y plane for three element spacings and the same operating frequency. Note that the E-plane pattern is no longer distorted and that the cross-polar component is not shown because it has been effectively reduced to well below -30 dB. In this case, the feed probes remained in the same plane and, as such, the cross-polar component did not increase as it did for the H-plane array. The H-plane pattern is essentially unchanged from that of the previous array. The self and mutual impedances for the array elements are shown in Fig. 11(a) and (b), respectively. Compare the mutual impedances of the array, which is driven out of phase to those of the in-phase array. Note that the slope of the curves for the mutual impedances is much greater than

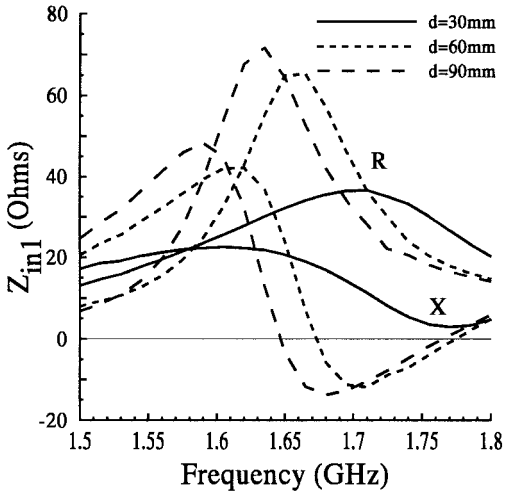

Fig. 12. Computed driving point impedances for various spacings d versus frequency for the antenna of Fig. 2(a) with $r_d = 24.5$ mm, $h = 39.5$ mm, $t = 0.0$ mm, $x_{f1} = x_{f2} = 0.0$ mm, $z_{f1} = -(33.5 + d/2)$ mm, $z_{f2} = (33.5 + d/2)$ mm, $V_{p1} = 1\angle 0°, V_{p2} = 1\angle 180°$.

the slope of the curves for the array with the distorted E-plane patterns. This is because in the latter case, the radiation due to coupling with the undesirable higher order modes, excited by the in-phase feed configuration, contributed to radiation over a greater range of frequencies. Finally, Fig. 12 plots the driving point impedances obtained from the impedance matrix elements presented in Fig. 11. Note that as the element spacing increases, the resonant frequency of the array decreases in a monotonic fashion apparently due to the fact that modes other than the dominant mode have been effectively eliminated.

IV. Summary

A rigorous numerical technique for the analysis of linear arrays of ground-plane-backed coaxial probe fed DR antennas has been presented. The self and mutual impedances determined using this technique for a two element DR array operating in the TE_{01} show good agreement with those obtained by measurements. Results of basic studies have been presented for DR arrays operating in the TE_{01} modes. Criteria for optimizing pattern performance based upon feed positioning and source phasing have been presented. This data can be used for meeting initial design criteria for large linear arrays since it concerns the effects of feed-probe position element spacing and port excitation upon the impedance and radiation characteristics of the antenna array.

Acknowledgment

The authors would like to thank the reviewers for their valuable comments.

References

[1] S. A. Long, M. W. McAllister, and L. C. Shen, "The resonant dielectric cavity antenna," *IEEE. Trans. Antennas Propagat.*, vol. AP-31, pp. 406–412, May 1983.

[2] M. W. McAllister and S. A. Long, "Resonant hemispherical dielectric antenna," *Electron. Lett.*, vol. 20, no. 3, pp. 657–658, Aug. 1984.

[3] A. W. Glisson, D. Kajfez, and J. James, "Evaluation of modes in dielectric resonators using a surface integral equation formulation," *IEEE Trans. Microwave Theory Tech.*, vol. MTT-31, pp. 1023–1029, Dec. 1983.

[4] D. Kajfez, A. W. Glisson, and J. James, "Computed modal field distributions for isolated dielectric resonators," *IEEE Trans. Microwave Theory Tech.*, vol. MTT-32, pp. 1609–1616, Dec. 1984.

[5] G. D. Loos and Y. M. M. Antar, "Investigation of a novel aperture couple dielectric resonator subarray," in *IEEE Antennas Propagat. Soc. Int. Symp. Dig.*, Seattle, WA, June 1994, pp. 1510–1513.

[6] G. P. Junker, A. A. Kishk, and A. W. Glisson, "Input impedance of dielectric resonator antennas excited by a coaxial probe," *IEEE Trans Antennas Propagat.*, vol. 42, pp. 960–966, July 1994.

[7] K. M Luk, W. K. Leung, and K. W. Leung, "Mutual impedance of hemispherical dielectric resonator antennas," *IEEE Trans. Antennas Propagat.*, vol. 42, pp. 1652–1654, Dec. 1994.

[8] Y. T. Lo and S. W. Lee, *Antenna Handbook: Theory, Applications, and Design*. New York: Van Nostrand Reinhold, pp. 35–49, 1988, ch. 14.

[9] G. P. Junker, A. W. Glisson, and A. A. Kishk, "Mutual coupling effects and radiation characteristics of a linear array of dielectric resonator elements fed by coaxial probe," in *IEEE Antennas Propagat. Soc. Int. Symp. Dig.*, Newport Beach, CA, July 1995, pp. 1998–2001.

[10] V. W. H. Chang and R. W. P. King, "On two arbitrarily located identical parallel antennas," *IEEE Trans. Antennas Propagat.*, vol. AP-16, pp. 309–317, May 1968.

[11] R. W. P. King, R. B. Mack, and S. S. Sandler, *Arrays of Cylindrical Dipoles*. Cambridge, MA: Cambridge Univ. Press, 1968.

[12] R. F. Harrington, *Time Harmonic Electromagnetic Fields*. New York: McGraw-Hill, 1961.

[13] L. N. Medgyesi-Mitschang and J. M. Putman, "Electromagnetic scattering from axially inhomogeneous bodies of revolution," *IEEE Trans. Antennas Propagat.*, vol. AP-32, pp. 797–806, Aug. 1984.

[14] A. A. Kishk and L. Shafai, "Different formulations for numerical solution of single and multibodies of revolution with mixed boundary conditions," *IEEE Trans. Propagat.*, vol. AP-34, pp. 666–673, May 1986.

[15] R. F. Harrington, *Field Computation by Moment Methods*. Malabar, FL: Krieger, 1968.

[16] A. A. Kishk, "Different integral equations for numerical solution of problems involving conducting or dielectric objects and their combination," Ph.D. dissertation, Univ. Manitoba, Manitoba, Canada, 1986.

[17] G. P. Junker, A. A. Kishk, and A. W. Glisson, "A novel delta gap source model for center fed cylindrical dipoles," *IEEE Trans. Antennas Propagat.*, vol. AP-43, pp. 537–540, May 1995.

[18] J. F. Schaeffer and L. N. Medgyesi-Mitschang, "Radiation from wire antennas attached to bodies of revolution: the junction problem," *IEEE Trans. Antennas Propagat.*, vol. AP-30, pp. 426–431, Mar. 1982.

[19] D. Kajfez, "Notes on microwave circuits," vol. 2, Univ. Mississippi, Oxford, MS, Kajfez Consulting, 1984.

[20] G. P. Junker, A. A. Kishk, and A. W. Glisson, "Numerical analysis of dielectric resonator antennas excited in quasi-TE modes," *Electron. Lett.*, vol. 29, no. 21, pp. 1810–1811, Oct. 1993.

[21] G. P. Junker, A. A. Kishk, A. W. Glisson, and D. Kajfez, "Effect of fabrication imperfections for ground-plane-backed dielectric resonator antennas with coaxial excitation," *IEEE Antennas Propagat. Mag.*, vol. 37, pp. 40–47, Feb. 1995.

Gregory P. Junker (S'88–M'95) was born in New Orleans, LA. He received the B.S. degree in electrical engineering from the University of New Orleans, LA, in 1979, the M.S. degree in electromagnetics from the University of Tennessee, Knoxville, in 1985, and the Ph.D. degree in electrical engineering from the University of Mississippi, University, in 1994.

In 1979, he joined Control Data Corporation's Advanced Design Lab, Arden Hills, MN, where his primary responsibility was that of designing CPU-based diagnostics for the Cyber 200 series supercomputer. From 1991 to 1995 he was Research Assistant, Research Associate, and an Instructor of electrical engineering at the University of Mississippi. He is currently with TRW, Redondo Beach, CA. His current research interests include the development of numerical techniques for open- and closed-region electromagnetic boundary value problems and optimization techniques applied to the design of antenna feeds, multibeam, and phased antenna arrays.

Dr. Junker was awarded the Doctor of Philosophy Achievement Award in engineering by the University of Mississippi in 1995.

Ahmed A. Kishk (S'84–M'86–SM'90–F'98) received the B.S. degree in electrical engineering from Cairo University, Egypt, in 1977, and in applied mathematics from Ain-Shams University, Cairo, Egypt, in 1980, and the M.Eng. and Ph.D. degrees from the Department of Electrical Engineering, University of Manitoba, Winnipeg, Canada, in 1983 and 1986, respectively.

From 1977 to 1981, he was a Research Assistant and an Instructor at the Faculty of Engineering, Cairo University. From 1981 to 1985 he was a Research Assistant at the Department of Electrical Engineering, University of Manitoba and from December 1985 to August 1986 he was a Research Associate Fellow there. In 1986 he joined the Department of Electrical Engineering, University of Mississippi, as an Assistant Professor. In the summer of 1989, he was a Visiting Research Scientist at the Royal Military College of Canada, Kingston, ON, Canada. He was on sabbatical leave at Chalmers University of Technology, Gothenburg, Sweden, during the 1994–1995 academic year. He has been a Professor at the University of Mississippi since 1995. He was an associate editor of *Antennas and Propagation Magazine* from 1990 to 1993 and is currently an editor of that publication. He was a co-editor of the special issue on "Advances in the Application of the Method of Moments to Electromagnetic Scattering Problems" in the *ACES Journal*. He has been an editor of the *ACES Journal* since March 1997. He has published over 195 journal and conference papers, technical reports, and patents. He is a co-author of *Microwave Horns and Feeds* (London, U.K.: IEE, 1994; New York: IEEE, 1994) and of Chapter 2 of the *Handbook of Microstrip Antennas* (Stevenage, U.K.: Peter Peregrinus, 1989). His research interests include the areas of design of millimeter frequency feeds for parabolic reflectors, dielectric resonator antennas, microstrip antennas, small antenna feeds for parabolic reflectors, mobile satellite antennas, phased array antennas, computer-aided design for antennas, numerical solutions of electromagnetic problems, and scattering from complex objects.

Dr. Kishk received the 1995 Outstanding Paper Award for a paper published in the *Applied Computational Electromagnetic Society Journal* and the 1997 Outstanding Engineering Educator Award from Memphis Section of the IEEE. He is a member of Sigma Xi Society, the U.S. National Committee of International Union of Radio Science (URSI) Commission B, the Applied Computational Electromagnetics Society, the Electromagnetic Academy, and Phi Kappa Phi Society.

Allen W. Glisson (S'71–M'78–SM'88) received B.S., M.S., and Ph.D. degrees in electrical engineering from the University of Mississippi, University, MS, in 1973, 1975, and 1978, respectively.

From 1973 to 1978, he served as a Research Assistant in the Electrical Engineering Department of the University of Mississippi. In 1978 he joined the faculty of the University of Mississippi, where he is currently Professor of Electrical Engineering. Since 1984, he has served as the associate editor for book reviews and abstracts for the *IEEE Antennas and Propagation Society Magazine* and has recently served as an associate editor for *Radio Science*. His current research interests include the development and application of numerical techniques for treating electromagnetic radiation and scattering problems and modeling of dielectric resonators and dielectric resonator antennas. He has been actively involved in the areas of numerical modeling of arbitrarily shaped bodies and bodies of revolution with surface integral equation formulations. He has also served as a consultant to several different industrial organizations in the area of numerical modeling in electromagnetics.

Dr. Glisson is a member of the Sigma Xi Research Society and the Honor Societies Tau Beta Pi, Phi Kappa Phi, and Eta Kappa Nu. He was selected as the Outstanding Engineering Faculty Member in 1986 and again in 1996. He is a member of four professional societies within the IEEE, Commission B of the International Union of Radio Science, and the Applied Computational Electromagnetics Society. He was a United States Delegate to the 22nd, 23rd, and 24th General Assemblies of URSI. He received the Ralph R. Teetor Educational Award in 1989. He received the Best Paper Award from the SUMMA Foundation and twice received a citation for excellence in refereeing from the American Geophysical Union. From 1991 to 1993 he served as the secretary of Commission B of the U.S. National Committee of URSI.